Rapid 3D light-sheet microscopy with a tunable lens

Fahrbach, F O ; Voigt, F F ; Schmid, B ; Helmchen, F ; Huisken, J

Abstract: The in-vivo investigation of highly dynamic biological samples, for example the beating zebrafish heart, requires high-speed volume imaging techniques. Light-sheet microscopy is ideal for such samples as it records high-contrast images of entire planes within large samples at once. However, in order to obtain images of different planes, it has been necessary to move the sample relative to the fixed focal plane of the detection objective lens. This mechanical movement limits speed, precision and may be harmful to the sample. We have built a light-sheet microscope that uses remote focusing with an electrically tunable lens (ETL). Without moving specimen or objective we have thereby achieved flexible volume imaging at much higher speeds than previously reported. Our high-speed microscope delivers 3D snapshots of sensitive biological samples. As an example, we imaged 17 planes within a beating zebrafish heart at 510 frames per second, equivalent to 30 volume scans per second. Movements, shape changes and signals across the entire volume can be followed which has been impossible with existing reconstruction techniques.

DOI: https://doi.org/10.1364/OE.21.021010

Rapid 3D light-sheet microscopy with a tunable lens

Florian O. Fahrbach, [1] **Fabian F. Voigt,** [2] **Benjamin Schmid** [1]
Fritjof Helmchen, [2] **Jan Huisken** [1,*]

[1] *Max Planck Institute of Molecular Cell Biology and Genetics, Pfotenhauerstrasse 108, 01307 Dresden, Germany*
[2] *Brain Research Institute, University of Zurich, Winterthurerstrasse 190, 8057 Zurich, Switzerland*
**huisken@mpi-cbg.de*

Abstract: The in-vivo investigation of highly dynamic biological samples, for example the beating zebrafish heart, requires high-speed volume imaging techniques. Light-sheet microscopy is ideal for such samples as it records high-contrast images of entire planes within large samples at once. However, in order to obtain images of different planes, it has been necessary to move the sample relative to the fixed focal plane of the detection objective lens. This mechanical movement limits speed, precision and may be harmful to the sample. We have built a light-sheet microscope that uses remote focusing with an electrically tunable lens (ETL). Without moving specimen or objective we have thereby achieved flexible volume imaging at much higher speeds than previously reported. Our high-speed microscope delivers 3D snapshots of sensitive biological samples. As an example, we imaged 17 planes within a beating zebrafish heart at 510 frames per second, equivalent to 30 volume scans per second. Movements, shape changes and signals across the entire volume can be followed which has been impossible with existing reconstruction techniques.

OCIS codes: (180.6900) Three-dimensional microscopy; (170.2520) Fluorescence microscopy; (170.1470) Blood or tissue constituent monitoring; (220.1080) Active or adaptive optics.

References and links

1. S. Ram, P. Prabhat, J. Chao, E. S. Ward, and R. J. Ober, "High Accuracy 3D Quantum Dot Tracking with Multifocal Plane Microscopy for the Study of Fast Intracellular Dynamics in Live Cells," Biophys. J. **95**, 6025–6043 (2008).
2. S. Abrahamsson, J. Chen, B. Hajj, S. Stallinga, A. Y. Katsov, J. Wisniewski, G. Mizuguchi, P. Soule, F. Mueller, C. Dugast Darzacq, X. Darzacq, C. Wu, C. I. Bargmann, D. A. Agard, M. Dahan, and M. G. L. Gustafsson, "Fast multicolor 3D imaging using aberration-corrected multifocus microscopy," Nat. Methods **10**, 60–63 (2012).
3. P. A. Dalgarno, H. I. C. Dalgarno, A. Putoud, R. Lambert, L. Paterson, D. C. Logan, D. P. Towers, R. J. Warburton, and A. H. Greenaway, "Multiplane imaging and three dimensional nanoscale particle tracking in biological microscopy," Opt. Express **18**, 877–884 (2010).
4. M. Levoy, Z. Zhang, and I. McDowall, "Recording and controlling the 4D light field in a microscope using microlens arrays," J. Mic. **235**, 144–162 (2009).
5. J. Huisken, J. Swoger, F. Del Bene, J. Wittbrodt, and E. H. K. Stelzer, "Optical sectioning deep inside live embryos by selective plane illumination microscopy," Science **305**, 1007–1009 (2004).
6. J. Huisken and D. Y. R. Stainier, "Selective plane illumination microscopy techniques in developmental biology," Development **136**, 1963–1975 (2009).
7. A. Kaufmann, M. Mickoleit, M. Weber, and J. Huisken, "Multilayer mounting enables long-term imaging of zebrafish development in a light sheet microscope," Development **139**, 3242–3247 (2012).

#192746 - $15.00 USD Received 24 Jun 2013; revised 13 Aug 2013; accepted 13 Aug 2013; published 30 Aug 2013

8. T. Panier, S. Romano, R. Olive, T. Pietri, G. Sumbre, R. Candelier, and G. Debrégeas, "Fast functional imaging of multiple brain regions in intact zebrafish larvae using Selective Plane Illumination Microscopy," Front. Neural Circuits **7**, 65 (2013).
9. T. F. Holekamp, D. Turaga, and T. E. Holy, "Fast Three-Dimensional Fluorescence Imaging of Activity in Neural Populations by Objective-Coupled Planar Illumination Microscopy," Neuron **57**, 661–672 (2008).
10. S. Kumar, D. Wilding, M. B. Sikkel, A. R. Lyon, K. T. MacLeod, and C. Dunsby, "High-speed 2D and 3D fluorescence microscopy of cardiac myocytes," Opt. Express **19**, 13839–13847 (2011).
11. C. Dunsby, "Optically sectioned imaging by oblique plane microscopy," Opt. Express **16**, 20306–20316 (2009).
12. E. J. Botcherby, R. Juškaitis, M. J. Booth, and T. Wilson, "An optical technique for remote focusing in microscopy," Opt. Commun. **281**, 880–887 (2008).
13. E. J. Botcherby, C. W. Smith, M. M. Kohl, D. Débarre, M. J. Booth, R. Juškaitis, O. Paulsen, and T. Wilson, "Aberration-free three-dimensional multiphoton imaging of neuronal activity at kHz rates," P. Natl Acad. Sci. USA **109**, 2919–2924 (2012).
14. J. Huisken and D. Y. R. Stainier, "Even fluorescence excitation by multidirectional selective plane illumination microscopy (mSPIM)," Opt. Lett. **32**, 2608–2610 (2007).
15. B. F. Grewe, F. F. Voigt, M. van't Hoff, and F. Helmchen, "Fast two-layer two-photon imaging of neuronal cell populations using an electrically tunable lens," Biomed. Opt. Exp. **2**, 2035–2046 (2011).
16. M. Liebling, A. S. Forouhar, R. Wolleschensky, B. Zimmermann, R. Ankerhold, S. E. Fraser, M. Gharib, and M. E. Dickinson, "Rapid three-dimensional imaging and analysis of the beating embryonic heart reveals functional changes during development," Dev. Dynam. **235**, 2940–2948 (2006).
17. C. Skupsch and C. Brücker, "Multiple-plane particle image velocimetry using a light-field camera," Opt. Express **21**, 1726–1740 (2013).

1. Introduction

The analysis of many interesting biological phenomena such as neuronal activity in the brain or blood flow in the heart requires the rapid recording of extended three-dimensional volumes. Established fluorescence microscopy techniques are not able to directly capture a three-dimensional volume all at once. Instead, images of different planes within the sample are captured sequentially, usually by moving the sample relative to the detection lens. This mechanical movement of the specimen or the lens limits acquisition speed, precision and may even be harmful to the sample. In order to capture the dynamic state of the sample and avoid distortions in the recorded data, volume imaging has to be performed by imaging multiple planes either in parallel or sequentially at very high speed, ideally without any sample movement.

Based on conventional fluorescence microscope setups, several methods for rapid simultaneous imaging of multiple planes have been developed in recent years. The most straightforward approach consists in using a set of cameras, each camera focused on a different plane [1]. This approach is only practicable for a low number of planes due to the low light efficiency and high complexity of such a multi-camera setup. Moreover, in general, objective lenses are corrected for one working distance so that the spacing of the planes has to be kept small. For large deviations from the ideal working distance the image quality deteriorates, especially due to spherical aberration.

Another approach makes use of the increasing sensor size of modern cameras: for example 9 planes were synchronously imaged onto adjacent regions on one sensor with a custom-made grating and prism for color-correction [2]. A simpler version based on a grating that is able to image 3 planes simultaneously was presented before [3]. Alternatively, by inserting a microlens array into the detection path of a conventional microscope, one can capture light fields of biological specimens in a single exposure, from which images of individual planes can be recovered [4].

The above-mentioned methods for multi-plane imaging are highly specialized: Number, size and spacing of the images are fixed for a given grating/prism combination or microlens array. Therefore the flexibility of such setups is limited and it is not possible to adapt the size of the field of view, the number of planes or the spacing quickly, e. g. during an experiment. Moreover, even though several, distinct planes are imaged at once, brightfield illumination exposes the

#192746 - $15.00 USD Received 24 Jun 2013; revised 13 Aug 2013; accepted 13 Aug 2013; published 30 Aug 2013

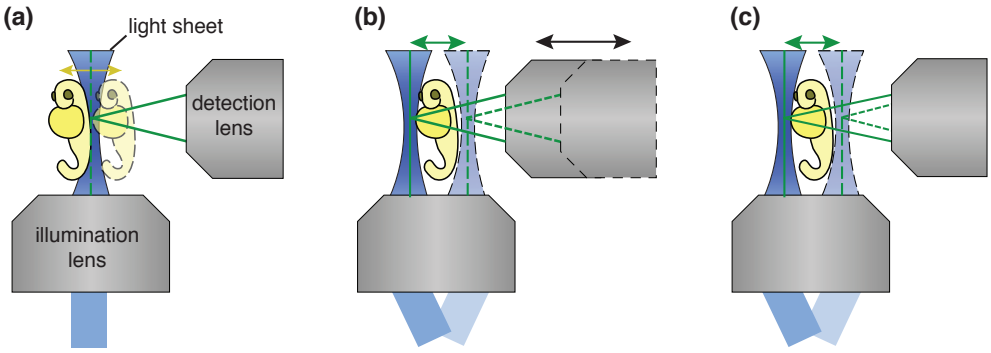

Fig. 1. **Three different approaches to volume imaging in SPIM.** (a) Volume image data in SPIM can be recorded by scanning the object through the stationary light sheet and aligned focal plane of the detection objective. Alternatively, the light sheet can be scanned through the sample by synchronized adjustment of the focal plane, either by repositioning the detection lens (b) or remote focusing (c), e.g. by a tunable lens to image the illuminated plane onto the camera.

entire sample to a light dose that is much larger than needed, which may result in bleaching of the fluorophores and photo-toxic effects.

Within the past decade, Selective Plane Illumination Microscopy (SPIM, [5]) has become recognized as an ideal tool for in-vivo imaging of biological specimens, e. g. for recording embryonic development in zebrafish (*Danio rerio*) and fruit flies (*Drosophila melanogaster*). SPIM offers optical sectioning, low photo-toxicity, high image acquisition speed and multi-view imaging [6]. For the purpose of high-speed volume imaging SPIM is particularly well suited because single planes can be quickly illuminated and imaged onto a fast camera. Despite the fact that SPIM is already widely used the challenge of fast multi-plane imaging has not been addressed yet.

2. Comparison of different approaches for volume imaging in SPIM

Extended three-dimensional volumes can be explored by light sheet microscopy in three different ways (Fig. 1): by moving the sample, by moving the light sheet and the detection lens together or by moving the light sheet and refocusing the detection optics remotely. To image different planes within a sample in a light sheet microscope the sample, which is mounted in a gel cylinder, is moved through the stationary light sheet (Fig. 1(a)). This approach poses problems due to the instability of the gel cylinder since gel concentrations have to be kept low to allow normal development of sensitive samples like embryos. Stability problems can be overcome by using transparent plastic tubes for mounting [7]. Nevertheless, accelerations of the sample necessary to achieve fast volume imaging should generally be avoided as they may adversely affect the sample. The speed of this approach is limited to a few volumes per second [8].

Instead, to avoid sample movement in volume imaging, the focal plane of the detection unit can be moved through the stationary sample while scanning the light-sheet to follow the focal plane and constantly keep it illuminated. For example, the detection lens can be mounted on a motorized-stage for fast displacement along the detection optical axis and the light-sheet scanned with a motorized mirror (Fig. 1(b)). The speed of this approach is limited by the inertia of the detection objective lens and this factor becomes more critical as cameras are becoming faster. Currently available piezo-electric focusing devices are optimized either for speed or

#192746 - $15.00 USD Received 24 Jun 2013; revised 13 Aug 2013; accepted 13 Aug 2013; published 30 Aug 2013

scan range and cannot cover ranges of several 100 microns at more than 10 Hz. For water immersion lenses the tight sealing between the lens and the chamber that holds the immersion medium has to be flexible enough to allow the lens to move freely along the detection axis. Most importantly, when water immersion lenses are used, the fast movement of the objective lens induces vibrations in the immersion medium that may affect the sample. By launching the light sheet from a fiber that was mechanically coupled to the detection lens, image stacks of brain tissue over a range of 250 µm were recorded in 2 s already a few years ago [9]. Using a motorized detection lens, imaging over a range of 38 µm at a speed of 21 volumes per second has been demonstrated [10]. The system was based on oblique plane illumination, where an inclined light sheet to illuminate the sample is launched by the detection lens itself [11].

An alternative to objective scanning is remote focusing using an optical relay system and a tunable optical element (Fig. 1(c)). Botcherby et al. proposed to use a second objective lens to focus the image onto a mirror that can be moved along the optical axis for rapid scanning of the focal plane [12]. Such a system is complex to build and align and not light efficient. The technique has, so far, been used predominantly in the illumination path of point-scanning two-photon microscopes to re-position the excitation focus along the optical axis [13].

The above-mentioned techniques are limited in speed or light-efficiency. Here, we report remote focusing with an electrically tunable lens (ETL) in the detection path of a light-sheet microscope. We first describe the experimental setup in section 3 and then investigate the optical performance and characterize the dynamic behavior of the ETL in sections 4 and 5. Based on these results, we demonstrate two modes for volume imaging: In one mode we performed large volume scanning at moderate speed (Section 6). The speed of this mode is slightly higher than what is achieved by object scanning but with the advantage that the sample can remain at a fixed position. In the other mode, we investigated high-speed scanning of smaller volumes at volume frequencies of up to 100 Hz, more than 10 times faster than previously reported (Section 7).

3. Experimental setup

We modified a basic SPIM setup to incorporate an ETL in the detection path for remote focusing and a motorized scan mirror in the illumination path to move the light sheet accordingly (Fig. 2). In the illumination path, the beam from a fiber-coupled laser source (SOLE-6, Omicron) is expanded and focused by a cylindrical lens to a line in the back focal plane (BFP) of the illumination lens (HCX APO L 10×/0.3 W U-V-I, Leica) [14]. To shift the light sheet rapidly along the detection axis, we inserted a motorized piezo mirror (PI-334.2, Physik Instrumente) in a plane conjugate to the BFP between the cylindrical lens and the illumination lens.

On the detection side, regular SPIM setups use a detection lens and a tube lens to image the illuminated plane onto a camera. We inserted two lenses with equal focal length f_r in a $4f$ configuration between the tube lens and the camera (Orca Flash 4.0, Hamamatsu). We placed an ETL (EL-10-30-C-VIS-LD, Optotune) between two relay lenses in a conjugate of the back focal plane of the detection lens (Fig. 2). Note that the ETL is a liquid lens and needs to be mounted in a horizontal orientation. Therefore, we included two mirrors to steer the detected light through the ETL (Fig. 2). The focal length of the ETL f_{ETL} determines the position of the plane that is imaged onto the fixed camera sensor. f_{ETL} spans approximately from 40 mm to 140 mm. To achieve symmetric displacement of the image plane around the native focal plane of the detection objective, the ETL is paired with an offset lens with $f_{\mathrm{OL}} = -75$ mm so that $1/f_{\mathrm{ETL,eff}} = 1/f_{\mathrm{ETL}} + 1/f_{\mathrm{OL}} - d/(f_{\mathrm{ETL}} \cdot f_{\mathrm{OL}}) \approx 1/f_{\mathrm{ETL}} + 1/f_{\mathrm{OL}}$. The displacement of the image plane is given by

$$\delta z_{\mathrm{det}} = -\frac{1}{M_{\mathrm{det}}^2} \cdot \frac{n f_r^2}{f_{\mathrm{ETL,eff}}}. \tag{1}$$

where n is the refractive index of the immersion medium. Note that an objective lens with half

#192746 - $15.00 USD Received 24 Jun 2013; revised 13 Aug 2013; accepted 13 Aug 2013; published 30 Aug 2013

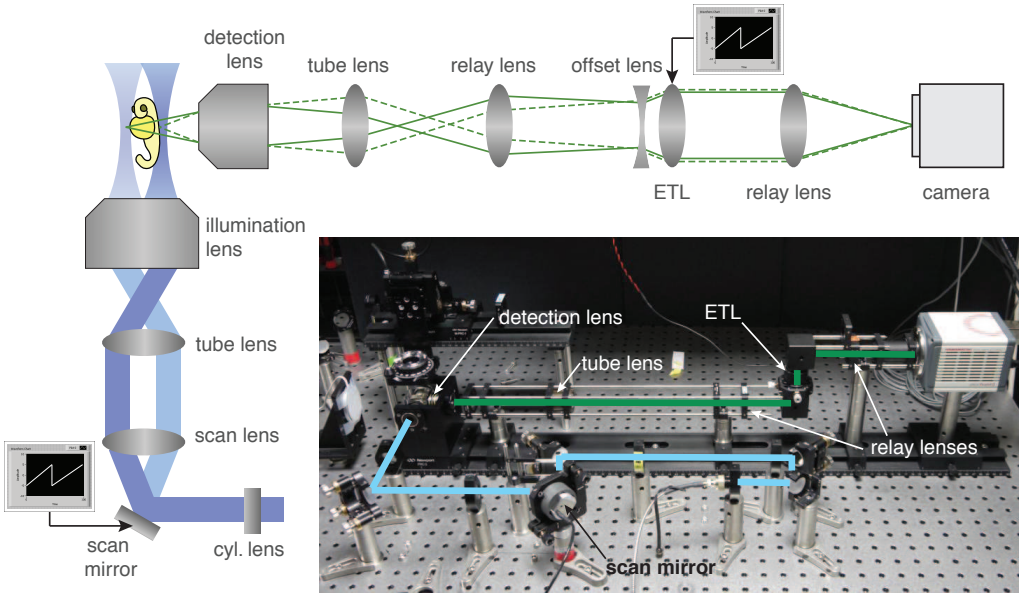

Fig. 2. **A SPIM setup has been modified to include a scan mirror and an ETL lens:** The light sheet is generated by focusing a line into the back focal plane of the illumination lens using a cylindrical lens. A motorized scan mirror displaces the light sheet along the detection optical axis. The image plane is displaced by changing the focal length of the ETL in-between the two relay lenses. Illumination light is shown in blue, fluorescence in green.

the magnification M_{det} will exhibit a four times larger scanning range for the same change in focal length of the ETL. The back focal plane of the detection lens is imaged onto the ETL by the tube lens and the relay lens in a $4f$ configuration. Due to the telecentricity of the setup, the magnification of the detection path does not depend on f_{ETL} and hence the displacement of the image plane δz_{det}. Generally, the scan range is proportional to the square of the focal length of the relay lenses f_{r}. However, there is an upper limit to f_{r}. To maintain the full NA of the detection lens, the ratio of the focal lengths of the relay lens f_{r} and the tube lens f_{TL} must not be larger than the ratio of the aperture of the ETL d_{ETL} and the diameter of the BFP of the detection lens d_{BFP}, i.e.

$$f_{\mathrm{r}} \leq f_{\mathrm{TL}} \cdot \frac{d_{\mathrm{ETL}}}{d_{\mathrm{BFP}}}. \tag{2}$$

Furthermore, precise alignment of the ETL is critical. The correct position of the ETL along the detection optical axis ensures that the magnification of the system is independent of the ETL's focal length f_{ETL}. The ETL has to be centered on the optical axis to avoid any lateral shift of the image in dependence of f_{ETL}. To align the lens we recorded images of a reference grid for the minimum and the maximum value of f_{ETL} and analyzed the lateral shift of the object's image. By repeating the process iteratively and adjusting the lateral position of the ETL the shift of the image can be eliminated.

#192746 - $15.00 USD Received 24 Jun 2013; revised 13 Aug 2013; accepted 13 Aug 2013; published 30 Aug 2013

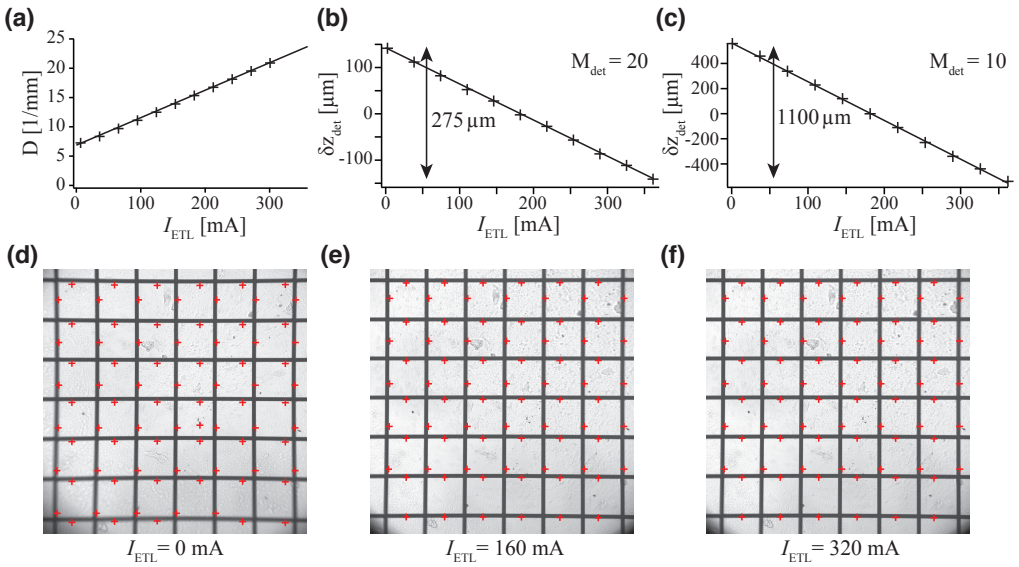

Fig. 3. **The ETL-SPIM setup exhibits a wide scan range and good image quality across almost the whole field.** (a) The ETL's refractive power $D_{\mathrm{ETL}} = 1/f_{\mathrm{ETL}}$ as a function of the applied current (measurement by Optotune AG). (b, c) The dependence of the position of the focal plane on currents I_{ETL} for the 10×/0.3 lens (b) and the 20×/0.5 lens (c). (d-f) A grating with a period of 100 µm imaged with a 20×/0.5 lens for three different currents: (d) $I_{\mathrm{ETL}} = 0$ mA, (e) $I_{\mathrm{ETL}} = 160$ mA, and (f) $I_{\mathrm{ETL}} = 320$ mA. The red crosses indicate the lower/right edge of the line that were located to measure the magnification and the distortion.

4. Imaging performance

To investigate the imaging performance of the ETL in our light-sheet microscope we addressed the following aspects:

1. How does the shift of the image plane depend on the ETL current?
2. How good is the image quality across the field of view in different image planes?

A transparent grid with a period of 100 µm was homogeneously illuminated with incoherent white light in transmission. We changed the image plane by applying different static currents I_{ETL} to the ETL and then moved the grid with a motorized stage (M-111.1DG, Physik Instrumente) to bring it into focus and precisely measure its axial position. The refractive power $D_{\mathrm{ETL}} = 1/f_{\mathrm{ETL}}$ is known to be linearly proportional to the current I_{ETL} (Fig. 3(a)). Therefore, we also expected a linear dependence between the shift of the image plane and the driving current. This assumption was confirmed with a relative precision better than 1% for both lenses that we used: a 10×-lens (HCX APO L 10×/0.3 W U-V-I, Leica) and a 20×-lens (HCX APO L 20×/0.5 W U-V-I, Leica). We measured the z-range and found values of 1.1 mm for the 10× lens (Fig. 3(b)) and 275 µm for the 20× lens (Fig. 3(c)). As expected, the range is inversely related to the square of the magnification of the detection lens.

We determined the magnification of the entire detection path by measuring the period of the grid in the image. For equidistantly spaced horizontal and vertical line profiles through the image the positions of the grid were automatically detected based on a threshold value of the derivative. These positions are marked by red crosses in Fig. 3(d)-(e). The relay system has

#192746 - $15.00 USD Received 24 Jun 2013; revised 13 Aug 2013; accepted 13 Aug 2013; published 30 Aug 2013

only a small influence on the magnification. For the lens with a nominal magnification of 20 we found $M = 17.9$ and for the $10\times$ lens we obtained $M = 9.0$. This small change of around 10% is caused by the Galilean telescope formed by the ETL and the diverging offset lens.

We also measured the distortion introduced by the relay system with the ETL as the ratio between the full width of 6 grating periods in the center and at the border of the image both vertically and horizontally. Using the $20\times$ detection lens, the distortion over a field of view as large as $750\,\mu\text{m} \times 750\,\mu\text{m}$ was only approximately 1% (Fig. 3(d)-(f)). For the $10\times$ lens we found comparable values.

Preliminary numerical studies had already revealed that the optical performance varies over the field of view and depends on the detection objective's numerical aperture NA_{det} and the wavelength range $\Delta\lambda$. Lower limits to aberrations were obtained by ray-tracing simulations. As a consequence, a relay system composed of two identical achromatic lenses with moderate focal length $f_{\text{r}} = 100\,\text{mm}$ was chosen. Thereby distortion, coma and lateral chromatic aberrations are kept to a minimum. Nevertheless, the images of defocused small fluorescent spheres reveal astigmatism that increases towards the borders of the image, where it also becomes more visible due to the field curvature. The latter is mainly introduced by the relay system even without the ETL. On the one hand, depending on the required image quality, aberrations may restrict the use of the system to a central region of the field of view. As the aberrations increase towards the limits of the ETL focal range, a reduction of the scan range also increases overall image quality. On the other hand, the aberrations introduced by the relay system and the ETL actually turn out not to be restrictive for many applications like cell tracking or shape measurements. Also, in some cases they are expected to be insignificant because diffraction-limited resolution cannot be achieved anyway due to strong scattering of the sample, e. g. zebrafish embryos.

5. The dynamic behavior of the ETL

Light-sheet microscopy generally requires the illumination plane to be perfectly coincident with the focal plane of the detection lens. Otherwise the recorded image is blurred. In conventional setups this overlap of the static light sheet and the image plane is maintained during the entire experiment after an initial alignment process. In our setup, the position of the light sheet z_{LS} and the image plane z_{det} are rapidly and independently adjustable to enable volume scanning. To ensure the overlap of illumination and detection at all times, the relationship between the signal driving the ETL, $I_{\text{ETL}}(t)$, and the signal driving the piezo mirror, U_{PM}, has to be determined so that $z_{\text{LS}} = z_{\text{det}}$ and the light-sheet follows the image plane during the scan.

The relationship will depend on the specifics of the setup: the ETL characteristics, magnification of the detection lens and focal length of the relay lenses. In general, our measurement procedure is applicable to almost all cases where illumination and detection have to be kept coincident.

First, we wanted to obtain precise knowledge of the time-dependent axial shift $\delta z_{\text{det}}(t)$ of the detection focal plane for specific, time-dependent steering currents $I_{\text{ETL}}(t)$. We used a sample consisting of a homogeneous distribution of small fluorescent spheres embedded in agarose gel to quantitatively analyze the overlap of the image plane and the light sheet. Illuminated beads only yield a large intensity in the image if they are located in the focal plane of the detection lens and imaged onto the smallest possible, ideally diffraction-limited, area on the camera sensor. Note that the measure of maximum image intensity requires a uniform distribution of single beads. The density of the spheres is very critical and clusters of spheres should be avoided as they may represent the brightest spots in an image even if they are out-of-focus.

First, the light-sheet position $z_{\text{LS}} = z_0$ is kept static and a varying current is applied to the ETL. At the same time, images $p(t)$ are recorded at the maximum available camera speed. From this series, the frame that shows the sharpest images of the fluorescent beads is determined.

#192746 - $15.00 USD Received 24 Jun 2013; revised 13 Aug 2013; accepted 13 Aug 2013; published 30 Aug 2013

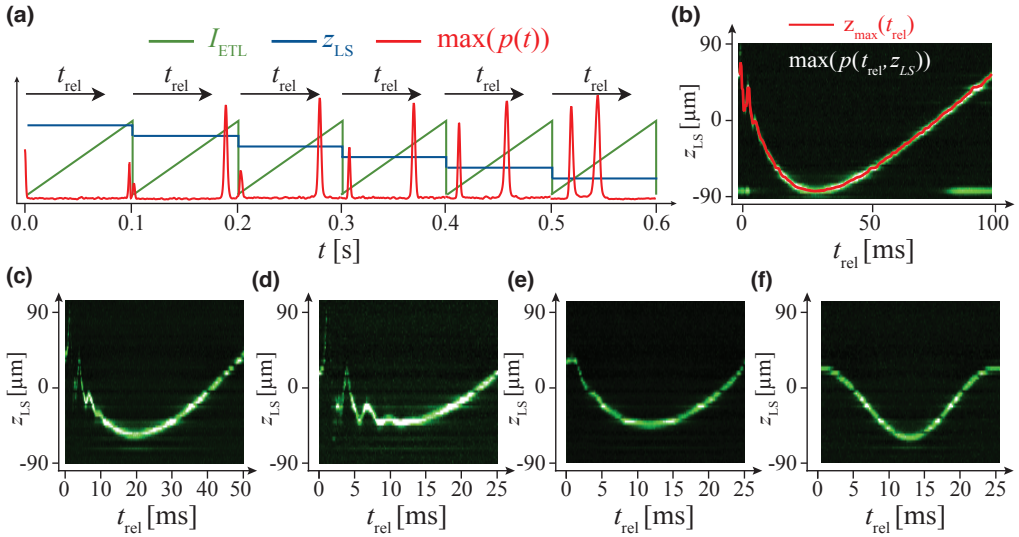

Fig. 4. **The dynamic behavior of the ETL in response to different driving signals.** (a) The image plane is scanned by applying a sawtooth current I_{ETL}. The maximum intensity of the image is shown in red. Peaks can be observed whenever the image plane and the light-sheet z_{LS} coincide. (b) The maximum value taken of the images $p(t)$ plotted against the position of the light-sheet z_{LS} and the time point within each ETL-period t_{rel}. The line at $-90\,\mu$m for $t_{\mathrm{rel}} \approx 0\,\mu$m and $100\,\mu$m is an artifact created by an out-of-focus cluster of spheres. (c-f) $\max(p(t_{\mathrm{rel}}, z_{\mathrm{LS}}))$ for sawtooth signals I_{ETL} at $\nu_{\mathrm{ETL}} = 20\,$Hz (c), $\nu_{\mathrm{ETL}} = 40\,$Hz (d), a lowpass-filtered sawtooth at $\nu_{\mathrm{ETL}} = 40\,$Hz (e) and a sine at $\nu_{\mathrm{ETL}} = 40\,$Hz (f).

In this frame (taken at the time t_c) the light-sheet and the image plane coincide. Because the position of the light-sheet z_0 is known, the position of the image plane at timepoint t_c is now also known to be $z_{\mathrm{ETL}}(t_c) = z_0$. In order to obtain more points in the $z_{\mathrm{ETL}}(t)$-curve, it is necessary to repeat this measurement for a series of light-sheet positions $z_{\mathrm{LS}} = z_0 + i\delta z$ with $i = 1 \ldots n$.

An example for such a measurement is shown in Fig. 4(a). We applied a sawtooth signal with frequency $\nu_{\mathrm{ETL}} = 10\,$Hz to the ETL. For each period, the light sheet was displaced in small steps $z_{\mathrm{LS}} = z_1, \ldots, z_6$. The camera recorded images $p(z_{\mathrm{LS}}, t_{\mathrm{rel}})$ of a small subregion of 128×64 pixel at the maximum framerate ($\nu_{\mathrm{cam}} = 3,200\,$Hz), hence, for each position of the light sheet z_{LS} a stack consisting of $\nu_{\mathrm{cam}}/\nu_{\mathrm{ETL}} = 320$ images was taken. The maximum intensity value of each frame $\max p(t)$ is also shown in Fig. 4(a). Peaks reveal the overlap of illumination and detection, i. e. the light-sheet and the image plane. One can already see from the positions of the peaks that the ETL did not follow the sawtooth-signal. Ideally, there would be two peaks in each ETL-period. A first peak near $t_{\mathrm{rel}} = 0$ indicates the overlap of light sheet and image plane during the sharp edge of the sawtooth. This peak should be very dim due to the high speed of the refocusing with the ETL. The second peak ideally shifts in steps of equal size from $t_{\mathrm{rel}} = 0.1\,$s in the first period to $t_{\mathrm{rel}} = 0\,$s. The magnitude of the first peak and the shift towards larger values t_{rel} indicate that the ETL is not able to follow the steep slope of the driving signal.

To investigate this behavior more closely, the measurement was repeated for $n = 100$ positions of the light-sheet with a very fine spacing δz_{LS}. Figure 4(b) shows the maximum intensity $\max p(t_{\mathrm{rel}}, z_{\mathrm{LS}})$ of each image. The position of the image plane $z(t_{\mathrm{rel}})$ can be derived from the maximum values $p(t_{\mathrm{rel}}, z_{\mathrm{LS}})$ for each t_{rel} and is indicated by a red graph in Fig. 4(b). Figure 4(c) and 4(d) were obtained for higher frequencies $\nu_{\mathrm{ETL}} = 20\,$Hz and $\nu_{\mathrm{ETL}} = 40\,$Hz, respectively. Driving the ETL with a sawtooth signal obviously leads to strong temporal oscillations

#192746 - $15.00 USD Received 24 Jun 2013; revised 13 Aug 2013; accepted 13 Aug 2013; published 30 Aug 2013

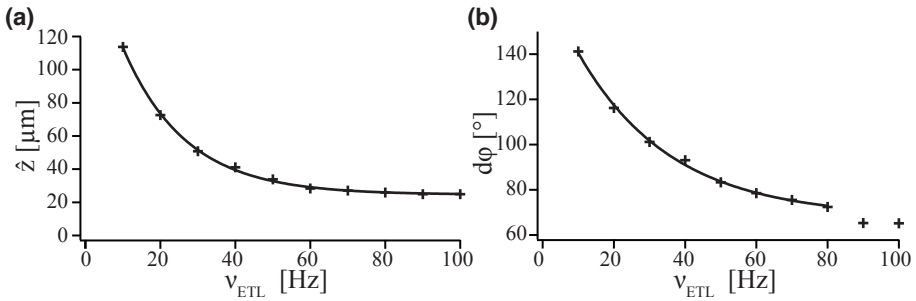

Fig. 5. **Frequency-dependent amplitude for the 20× objective and phase of the focal length of the ETL.** The amplitude (a) and the phase shift (b) of the axial position of the image plane. The ETL was driven with a sinusoidal signal. The crosses mark measurement results. Exponentially decaying functions were fitted to the data.

of its focal length. The reason for this effect is the resonant behavior of the ETL: The temporal spectrum of the ETL exhibits two broad resonance peaks around 300 Hz and 600 Hz [15]. Due to this overshooting only a small part of each period can actually be used to reliably record an image stack. It is therefore mandatory to avoid high-frequency components in the driving signal $I_{\mathrm{ETL}}(t)$.

We first tried low-pass filtering of the sawtooth signals. Figure 4(e) shows the result for $\nu_{\mathrm{ETL}} = 40\,\mathrm{Hz}$ and a cutoff frequency of 200 Hz. One can clearly see that the overshoot was reduced. However, the $z_{\mathrm{ETL}}(t)$-curve is strongly nonlinear which makes it difficult to move the light-sheet accordingly. We found that sinusoidal driving signals were best for rapid volume imaging in a light sheet microscope with our ETL. When driving the ETL with sinusoidal signals, the position of the detected plane smoothly followed a sinusoidal curve, too (Fig. 4(f)).

To measure the frequency-dependent amplitude and the phase of the position of the image plane z_{ETL} we fitted sine functions to the maximum signal $z_{\max}(t_{\mathrm{rel}})$ for several frequencies f_{ETL} from 10 Hz to 100 Hz. The full peak-to-peak amplitude decayed from 240 µm for $\nu_{\mathrm{ETL}} = 10\,\mathrm{Hz}$ to values around 80 µm for $\nu_{\mathrm{ETL}} = 100\,\mathrm{Hz}$ for the 20× detection lens (Fig. 5(a)). The phase shift decreased exponentially from 140° to 70°(Fig. 5(b)). For drive signals at 90 Hz and 100 Hz the measurement of the phase was not reliable anymore due to the difficulty of precisely fitting a sine function even though several periods were recorded.

Note that the piezo mirror used in our setup shows a decrease in amplitude at higher driving frequencies. Therefore, we performed the measurement described above also after exchanging the driving signals, i. e. sine signals were applied to the mirror while the ETL-current was changed step-wise after each period to shift the focal planes. Using this method for the motorized mirror, the small frequency delay and the decrease in amplitude for higher frequencies could be quantified. Alternatively, a faster galvanometric scanning mirror could be used to position the light sheet for high speed volume imaging with an ETL.

6. Large volume scan

In this section we demonstrate as a first application mode how an ETL can be used to image large volumes. Special care has to be taken when the resonant behavior of the ETL starts to dominate the focusing dynamics as the ETL always reacts with a certain delay. In these experiments the goal was to run the ETL at the highest speed that still allowed to use the full amplitude as measured in Figs. 3(b) and 3(c). For our ETL, this volume scanning frequency was limited by $\nu_{\mathrm{ETL}} \approx 10\,\mathrm{Hz}$, which is still faster than what can be readily achieved for comparable ranges

#192746 - $15.00 USD Received 24 Jun 2013; revised 13 Aug 2013; accepted 13 Aug 2013; published 30 Aug 2013

with other methods such as moving the objective lens or the sample.

A stack can be acquired by displacing the image plane in small steps and taking a snapshot at each position. To keep the light sheet in the image plane, the mirror voltage U_{PM} once again needs to be calibrated to the ETL current I_{ETL}. Since the relationship between the ETL current I_{ETL} and the shift of the image plane δz_{det} is linear (Figs. 3(b) and 3(c)) the relation $U_{\mathrm{PM}}(I_{\mathrm{ETL}})$ can be interpolated from two measurements of $(U_{\mathrm{PM}}, I_{\mathrm{ETL}})$ that provide sharp images. Ideally these two planes are located at opposite ends of the desired z-range.

When the focal length of the ETL is changed in such a step-wise fashion the image has to be taken only after the ETL relaxed to the new focal length to obtain thinnest optical sections. This time delay limits the volume imaging speed. We measured the step response time of our ETL and found that it took 30 ms for steps over the full range and 5-15 ms for very small changes (1% of the ETL's full range). Therefore, the image acquisition rate is limited to 60 Hz for small steps and 30 Hz for large steps.

Higher speeds can be achieved when a continuous ramp signal is applied to the ETL that slowly changes the focal length according to $z_{\mathrm{det}} = z_{0,\mathrm{det}} + \mathrm{d}z_{\mathrm{det}}/\mathrm{d}t \cdot t$. The position of the light-sheet $z_{\mathrm{LS}} = z_{0,\mathrm{LS}} + \mathrm{d}z_{\mathrm{LS}}/\mathrm{d}t \cdot t$ has to change accordingly so that $z_{\mathrm{det}} = z_{\mathrm{LS}}$ at all times. Therefore, the offset $z_{0,\mathrm{det}}$ and the slope $\mathrm{d}z_{\mathrm{det}}/\mathrm{d}t$ have to be adjusted as described above. In this case, the axial spacing of the acquired planes is limited only by the camera speed.

The only disadvantage of the continuous ramp mode is that the image plane changes while the camera records an image which leads to thicker optical sections. This problem can be eliminated by pulsing the illumination for a short time during the exposure of the camera. The driving signals for the ETL and the scan mirror are shown together with the illumination trigger in Fig. 6(a). For best performance, the sample should be illuminated only within a time t_{flash} during which the image plane is shifted by less than the depth of field of the detection optics.

Pulsed illumination can also be useful for cameras with a rolling shutter (e.g. the Hamamatsu Orca Flash 4.0 used in our setup or comparable sCMOS cameras). In this case, the sample needs to be illuminated while the whole camera sensor is exposed. Otherwise, the rolling shutter will introduce artifacts, i. e. the camera records images of planes that are tilted with respect to the image plane. Obviously, this problem is not specific to the use of an ETL but to all high-speed volume imaging techniques with a continuous movement of the image plane relative to the sample. Due to the fast and efficient collection of fluorescence in light-sheet microscopy flashing the laser light represents a solution that can be easily implemented, even for multi-directional illumination (mSPIM, [14]): Ideally, the flash from one side is triggered at the end of one exposure and the flash from the other side at the beginning of the following exposure. In global shutter mode these two pulses can be fired with minimal delay.

In order to record image stacks always starting with the same plane, the ETL needs some time after each ramp to relax to the initial focal length. As explained before, a full amplitude step takes approximately 30 ms with an ETL. During this time, no images of well-defined planes can be acquired. However, at frequencies $f_{\mathrm{ETL}} \leq 5\,\mathrm{Hz}$ this time accounts for less than 15% of the period so that the duty cycle is ca. 85% of the period.

As a demonstration that two-color volume imaging of large samples is possible, Fig. 6 shows images of the vascular system in a zebrafish recorded with the 10×/0.3 lens. The transgenic fish Tg(kdrl:EGFP, GATA1:dsRed) expresses EGFP in its vasculature (green) and dsRed in its blood cells (red, Fig. 6). Additionally, Media 1 shows a three-dimensional rendering. A series of 150 images was acquired over a range of 330 µm for both colors separately. The spacing between planes was 2.2 µm. The stack was recorded in 3 s at 50 fps where and the laser was flashed for 10 ms during the time that the entire chip was exposed as indicated in Fig. 6. The laser powers delivered to the sample were approximately 3 mW at 488 nm and 2 mW at 561 nm. The ETL current was varied in continuous ramp mode from ≈ 90 mA to ≈ 210 mA.

#192746 - $15.00 USD Received 24 Jun 2013; revised 13 Aug 2013; accepted 13 Aug 2013; published 30 Aug 2013

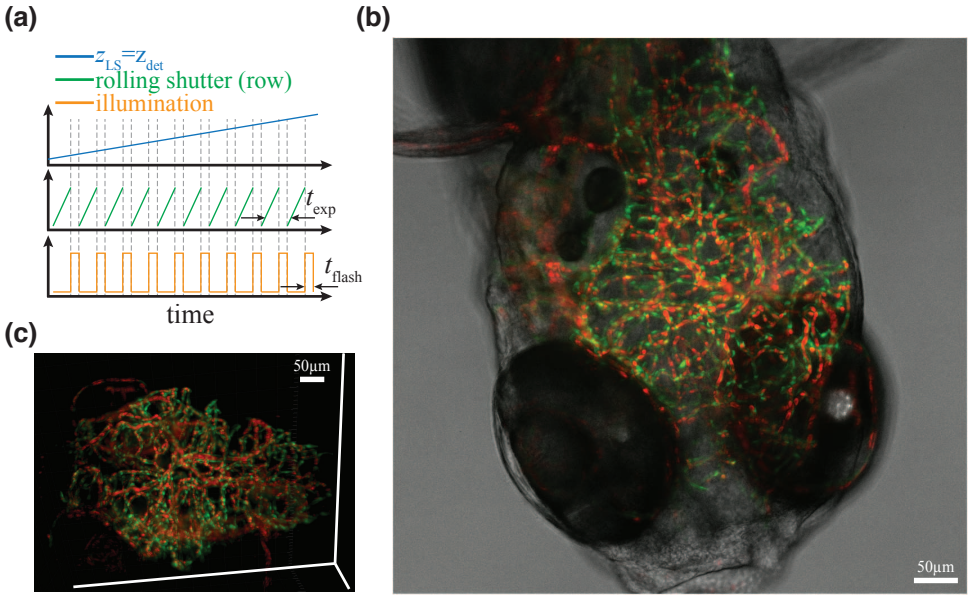

Fig. 6. **Large volume scan with an ETL through the head of a zebrafish (Media 1).** (a) Slowly varying ramp signals can be used for remote scanning through large volumes. Thin optical sections are recorded by flashing the illumination only for a short time when the rolling shutter exposes the full camera chip. (b,c) A stack of images of the vascular system in the brain of a zebrafish imaged by remote scanning (blood cells in red, vasculature in green). The figure shows a maximum projection along the detection axis overlaid with a bright-field image (b) and a three-dimensional rendering (c) which is also shown in Media 1. The data was recorded with the 10× lens.

7. High-speed volume scan

Section 5 showed measurements that provide precise knowledge of the time-dependent shift δz_{det} of the image plane for quickly varying driving signals. By sending this position information to the scan mirror it is in principle possible to illuminate the image plane with the light sheet over the entire period $1/\nu_{\mathrm{ETL}}$. However, we found that this method does not directly lead to satisfactory image quality and a more elaborate calibration method turned out to be necessary.

7.1. Dynamic Calibration

Additional calibration is necessary for the following reasons: First, the position of the image plane cannot be inferred from the measurements presented in section 5 with sufficient precision. The limit is set by the thickness of the light sheet and the frame rate of the camera even though it is already very high at several thousand frames per second. Second, the piezo scanning mirror has a low resonance frequency and therefore does not follow the driving signal at high frequencies as precisely as needed. Even though the mirror's response can also be measured and compensated for as described in section 5, to ensure the best possible match of the light sheet and the image plane, we performed a dynamic calibration after having measured the response of both the scan mirror and the ETL.

The dynamic calibration method consists in recording image stacks while applying dynamic driving signals to both the ETL and the mirror synchronously, just as one would do for a regular

#192746 - $15.00 USD Received 24 Jun 2013; revised 13 Aug 2013; accepted 13 Aug 2013; published 30 Aug 2013

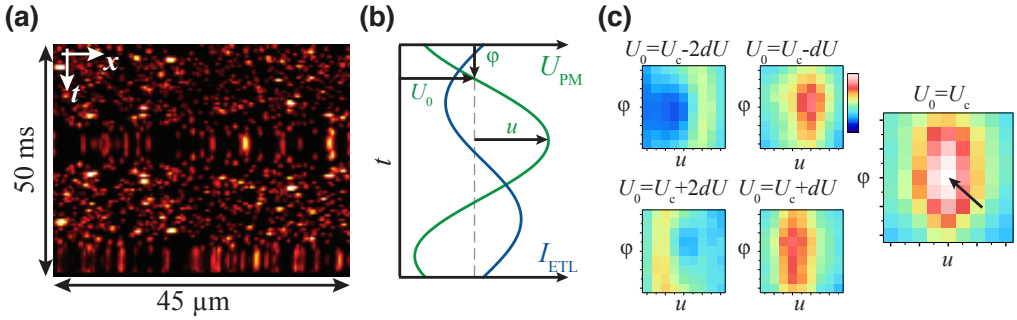

Fig. 7. **Dynamic calibration ensures perfect overlap of the light sheet and the image plane over the full period for high-speed volume scans (Media 2).** (a) Maximum projection of the image stack across the light sheet axis y over one period. Media 2 shows the full images. (b) Driving signals for the ETL, I_{ETL}, and the piezo-mirror U_{PM}. (c) Quality parameter $\bar{Q}_j$ that measures the overlap over one period for different parameters u_j and ϕ_j grouped in five subsets depending on the offset $U_{0,j}$ which is changed in steps dU. The maximum value is reached for $U_0 = U_c$, $\phi = \phi_c$ and $u = u_c$ and marked by an arrow. The image stack shown in (a) was recorded with these parameters. The data was recorded with the 20× lens.

measurement but at a much higher acquisition rate. For calibration, the parameters of the scan mirror signal (e.g. for a amplitude, offset and phase) are varied systematically relative to the ETL driving signal, which remains unchanged. The recorded image stacks are evaluated to find the ideal set of parameters that delivers best image quality throughout the entire image stack acquired during one ETL period.

The evaluation of the overlap between illumination and detection over the whole ETL-period i. e. across the recorded image stacks is critical: First, the overlap of light sheet and image plane has to be measured for each frame taken at time t with a particular set of parameters j. As discussed above, when beads are used, the maximum intensity within a single image p is a reasonable measure so that $Q_j(t) = \max_{\mathrm{x,y}} p_j(t)$. Higher moments of the image intensity like the kurtosis can be more robust measures. Second, the measures of the single images $Q_j(t)$ recorded over an entire period of the ETL need to be combined to give an overall score $\bar{Q}_j$ attributed to the respective set of parameters j. In general, taking the sum of the image maxima $\bar{Q}_j = \sum_t Q_j(t)$ over the entire period works well. The set of parameters that yields the highest $\bar{Q}_j$ is very likely to provide the best overlap of illumination and detection across the ETL-period. Since the overlap needs to be equal over the entire image stack, it can be useful to also evaluate the standard deviation of the $Q(t)$-values over the period $\bar{Q}_j = \mathrm{sdev}_t\, Q_j(t)$. Here, the set of parameters providing minimum $\bar{Q}_j$ would be the best, because the images taken within a period all reveal very similar signal strength, i. e. the maximum intensity of the images is even across the period. We found a combination of the different measures to be most reliable: a high sum indicates a good general overlap and a low standard deviation makes sure that the overlap is good over the whole period.

An example for a sinusoidal driving signal with $\nu_{\mathrm{ETL}} = 20\,\mathrm{Hz}$ and amplitude $\hat{z} \approx 70\,\mu\mathrm{m}$ is shown in Figure 7. In the projection of a recorded image stack along the axis of the light sheet, shown in Fig. 7(a), one can see that the bead images are equally bright in each frame which indicates the good overlap over the entire period. Media 2 shows a video of the full images over one period and further demonstrates the good image quality. For the employed sinusoidal driving signals $U_{\mathrm{PM}} = U_0 + u \cdot \sin\{2\pi\nu t + \phi\}$ three parameters required adjustment:

#192746 - $15.00 USD Received 24 Jun 2013; revised 13 Aug 2013; accepted 13 Aug 2013; published 30 Aug 2013

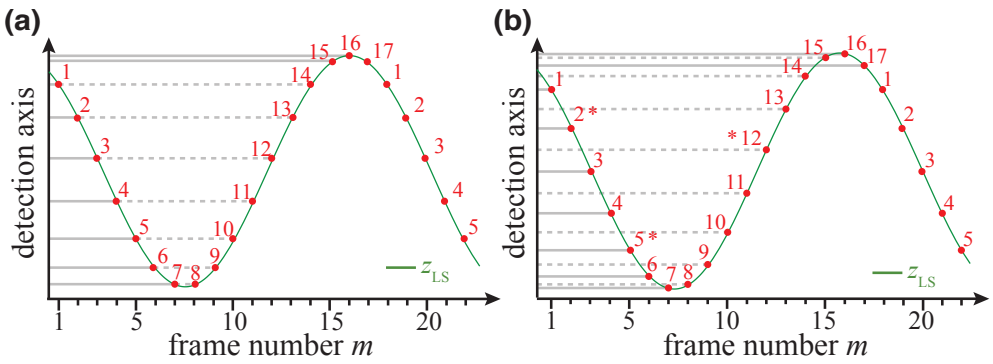

Fig. 8. **Sinusoidal driving signals offer two possibilities to increase either spatial or temporal sampling.** The green plot indicates the position of the image plane along the optical axis (vertical axis) over time (horizontal axis). The camera records images with constant temporal spacing. The timepoints are marked by red dots and the number i of the frame within the ETL period. m indicates the overall number of frames. In the two cases shown, either: (a) Each plane is imaged twice during each period, e.g. $i = 1$ and 14, $i = 2$ and 13, ..., or (b) planes imaged in the second half are lying between the planes imaged in the first half of each period.

The offset U_0, amplitude u and the phase ϕ of the mirror's driving signal were changed by small amounts in a systematic way to find the set of parameters that yielded sharp images of the sample during the entire period (Fig. 7(b)). Figure 7(c) shows the measured overlap $\bar{Q}_j$ over one period for different values of the offset, amplitude and phase. Using this dynamic calibration we could find a well-suited set of parameters ideally within a few minutes. In general we had to use 5 values for each parameter (U_0, u, and ϕ) which means we had to record and evaluate $j = 1 \ldots 125$ image stacks and perform several iterations where the intervals between the values of the different parameters (U_0, u, and ϕ) were reduced. Note that for sinusoidal driving signals we could not optimize the three parameters separately. From Fig. 7(c), one can see that the correct phase ϕ and amplitude u cannot be found unless the correct offset U_c is chosen.

7.2. Image Spacing

High-speed volume scanning using an ETL is performed best using sinusoidal signals in order to control the resonant behavior of the ETL. Therefore the spacing of the recorded planes is not equal throughout the acquired stack. However, it is well defined and known from the calibration curve (Fig. 5(g)). Taking this into account in post-processing, the data can nevertheless generate accurate volume images. Approximately 94% of the images are separated by more than 5% of the total amplitude and therefore contain information from different planes. Only a minor fraction of the images is acquired at the turning points.

When using sinusoidal signals, the user can choose between doubling either temporal or spatial sampling. Setting the relative phase of the camera trigger allows to choose between the two modes: Either the same plane is imaged once during the rising and once during the declining part of the sine thus doubling temporal sampling, or different planes are imaged during the two halves of each period to double the spatial sampling. Figure 8 sketches the two options to synchronize the volume scanning to the image acquisition when 17 images are recorded during one ETL period.

The first option is sketched in Fig. 8(a). where, for example, images 1 and 14 were taken at the same plane so that each plane is sampled twice during the ETL period. However, the time

#192746 - $15.00 USD Received 24 Jun 2013; revised 13 Aug 2013; accepted 13 Aug 2013; published 30 Aug 2013

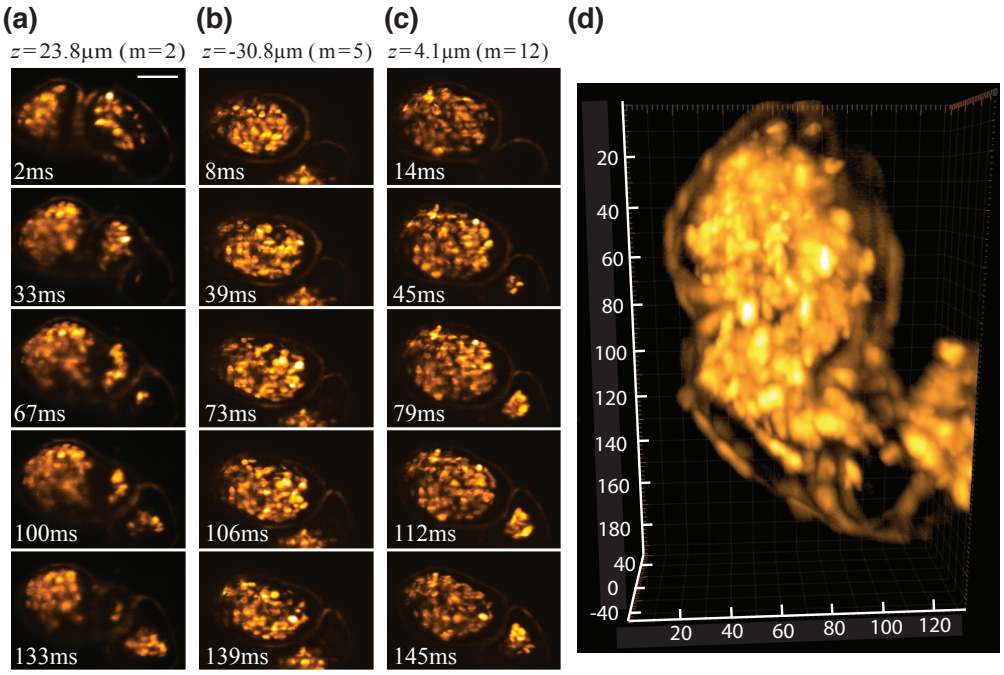

Fig. 9. **Movies of multiple planes in a beating zebrafish heart can be acquired synchronously (Media 3 & 4).** (a,b,c) Three series of images taken in different planes. The temporal spacing between two frames taken in the same plane is $1/f_{\mathrm{ETL}} = 1/30\,\mathrm{s}$. The corresponding movie is available as Media 3. The relative positions of the planes along the detection axis z can be inferred from Fig. 8(b) where the corresponding frames are marked by *. Scalebar: 50 µm. (b) A three-dimensional reconstruction. Units are microns. The corresponding movie is available as Media 4).

interval between two images taken in the same plane is not equal across the stack. The planes closer to the center of the stack are imaged more evenly at twice the volume scan frequency than the marginal planes. Of course this has to be accounted for in post-processing for critical applications like tracking of particles for speed measurements.

Second, the camera might be triggered such that different planes are imaged during the two halves of each period as shown in Fig. 8(b). Here the phase difference is equal to $\phi_{\mathrm{cam}} = \pi/\nu_{\mathrm{cam}}$ to make sure that the planes imaged in the second half of the period lie exactly in the center between the planes imaged in the first half of the period. All planes are imaged at the volume scanning frequency ν_{ETL} but with a different phase.

7.3. Example application: Imaging a beating zebrafish heart

Live imaging of the beating heart is of great interest to answer a number of fundamental questions on its development and function. Therefore, methods have been developed to synchronize images in post-processing [16]. These rely on data taken over a number of periods that are fused computationally. While these methods allow to infer structure and shape they are unable to yield information on dynamic parameters such as the blood flow. In contrast, an ideal imaging system can freeze the motion of the heartbeat by taking an image of the whole volume in an instant. The heart of the zebrafish is approximately 200 µm across and beats at 2-3 Hz. To freeze the motion the volume imaging rate has to be much larger than the heart-rate. As described in

#192746 - $15.00 USD Received 24 Jun 2013; revised 13 Aug 2013; accepted 13 Aug 2013; published 30 Aug 2013

section 1, at such speeds object scanning is not sensible anymore.

Using our ETL-SPIM setup we imaged a beating zebrafish heart. The transgenic fish *Tg(myl7:dsRed, GATA1:dsRed)* expressed *dsRed* in its blood cells and in the heart muscle cells. To image the whole heart at a magnification of $M_{\mathrm{det}} = 20$ the camera was cropped to a subregion of 600 × 408 pixels (equivalent to a FOV of 218 µm × 148 µm) to record images at a framerate of $\nu_{\mathrm{cam}} = 510\,\mathrm{Hz} = 17\,\nu_{\mathrm{ETL}}$. We excited dsRed at 561 nm with a total power of the light sheet of approximately 3 mW. The frequency of the ETL ν_{ETL} determines both the number of planes across the heart and the framerate at which each individual plane is imaged. The ETL was driven with a sine-signal at a frequency of $\nu_{\mathrm{ETL}} = 30\,\mathrm{Hz}$ so that 17 images were acquired during each period of the ETL. The movies of these planes are shown in Media 3. We chose to synchronize the camera to obtain a better spatial sampling as described in the previous section. The acquired images were sorted to generate 17 movies of different planes, each running at the framerate $\nu_{\mathrm{ETL}} = 30\,\mathrm{Hz}$. This means that the full heart was imaged approximately 15 times during each single heartbeat. The first 5 frames recorded from three different planes are shown as an example in Fig. 9(a). The position of the recorded planes is marked by * in Fig. 8(b). It can be seen that the framerate for each plane is fast enough to track changes in the morphology. In the three-dimensional rendering (Fig. 9(b) and Media 4) one can discern individual blood cells and follow their movement in the beating heart. As the volume images are taken within a single heartbeat, i.e. several planes are imaged nearly simultaneously, flow profiles can be created by determining the position of individual cells and tracking them over time.

8. Discussion

Previous methods for volume imaging had shown limitations regarding speed, flexibility or light-efficiency. In this paper, we inserted an electrically tunable lens in the detection arm of a light-sheet microscope for fast volume imaging without displacement of the sample. One of the major concerns regarding tunable lenses is image quality. We could find only minor aberrations in the image center, but more prominent astigmatism and coma increasing with the distance to the image center. Field curvature is also apparent, but it is mainly produced by the achromatic relay lenses. As the image quality depends on the focal length of the ETL and deteriorates towards the borders of the image, the effectively usable field of view (FOV) and scan range depend on the specific image quality requirements. In our setup, the point-spread function (PSF) is undersampled in order to increase the usable FOV which means that it was not possible to quantify the change of the PSF with respect to the detection wavelength range, distance to the optical axis and axial focusing range. With a 10×/0.3 objective and a wavelength range suitable for detecting GFP emission, the system can be expected to be diffraction-limited for a FOV of 600 µm over a z-range of 250 µm. We noted that the system provides excellent image quality that is sufficient for many applications far beyond this conservative estimate due to the undersampling of the PSF. Additionally, achieving diffraction-limited imaging performance when imaging deep inside living zebrafish embryos is usually impossible due to tissue aberrations.

The challenge to volume imaging in a light-sheet microscope by remote focusing is the desired overlap of the light sheet and the focal plane of the detection lens, which are both moving. In contrast, when rapidly shifting the image plane with an ETL in a point-scanning two-photon microscope [15], the image is in focus regardless of drift or any other effects. Calibration is needed only to know the absolute position of the excitation focus.

We successfully developed a straight-forward calibration routine that ensures perfect overlap of the light sheet and the image plane at all times even for highly dynamic driving signals up to frequencies of 100 Hz. The calibration relies on extremely fast image acquisition on a small central subregion using a small sample consisting of small fluorescent spheres. The limitation to a volume rate of 100 Hz was therefore imposed by the available fluorescence of the sample

#192746 - $15.00 USD Received 24 Jun 2013; revised 13 Aug 2013; accepted 13 Aug 2013; published 30 Aug 2013

and the speed of the camera.

Calibration during long-term measurement might be necessary when the ETL shows drift, i. e. the relationship between current and focal length is not constant over time. In general, the ETL is quite robust concerning such drift as long as the mean current applied to the lens is kept constant. The relationship between focal length and current is sufficiently stable over time. However, the absolute focal length for a given current changes with the temperature of the lens. Newly developed ETLs should therefore include a control unit that corrects for thermal drift.

Remote scanning with an ETL in a light-sheet microscope is currently the most light efficient method for fast volume imaging. The planes are imaged sequentially so that all fluorescence captured originates from the region illuminated by the light sheet. Even if multiple planes are illuminated by separate sheets of light [17], parallel imaging means that the fluorescence is shared between the images and moreover every illuminated plane contributes background to the other images.

Another advantage of the ETL-SPIM is its high flexibility compared to other volume imaging techniques. The number of images, their size and spacing along the optical axis can be varied even during the experiment. For high speeds a calibration has to be performed for different amplitudes or frequencies. We measured the overlap of the light sheet and the image plane in a dedicated sample composed of fluorescent spheres at high density. Therefore the calibration would have to be performed before the measurement. However, the calibration should ideally be performed directly within the sample. With autofocusing routines that work in any sample one could perform the calibration during the experiments without manual interaction.

In principle, the scan range is limited by the focal length range of the ETL. However, the scan range can be increased by using relay lenses with larger focal length. To be able to retain the usability of the full NA of the detection lens, the diameter of the ETL has to correspond to the back focal plane of the detection objective magnified by a telescope composed of the tube lens and a relay lens. Currently available ETLs feature apertures of 10 mm, whereas the diameter of the BFP of high-end detection lenses lies in the range between 20 mm and 25 mm. Therefore, the development of ETLs with a larger ratio of focusing range to clear aperture will be beneficial for application in SPIM.

When sinusoidal driving signals are used, one could also benefit from an increased amplitude when driving the ETL close to the resonance frequency. Currently the lower resonance peak of the ETL is located around 300 Hz [15], which is too fast for volume imaging. Even though it would be desirable to suppress the resonances altogether, there might be the option to lower the ETL resonance frequency by a modification of its design.

9. Summary

By including an electrically tunable lens in the detection arm of a light-sheet microscope, we were able to image extended three-dimensional volumes quickly with a highly flexible microscope setup. Using a $10\times/0.3$ lens a depth of more than 1 mm can be covered along the detection axis at frame rates up to several Hz. For higher volume frequencies in the range 20 Hz to 100 Hz sinusoidal driving signals are more suitable due to the dynamic behavior of currently available ETLs, which then reduces the achievable scan range. The inclusion of a remote focusing unit into a light sheet microscope unleashes the full potential of modern high-speed cameras and leaves the sample unaffected from any mechanical motion. Our ETL-SPIM is ideally suited for the rapid recording of transient signals, e. g. neuronal activity in the brain, and for the reconstruction of the blood flow in the heart. We expect that ETLs with larger apertures and better dynamic focusing performance will be available in the near future and render SPIM an even more powerful tool for high-speed volume imaging of living samples.

#192746 - $15.00 USD Received 24 Jun 2013; revised 13 Aug 2013; accepted 13 Aug 2013; published 30 Aug 2013

Acknowledgments

We thank Michaela Mickoleit and Michael Weber for the preparation of Zebrafish samples. Michael Weber rendered the three-dimensional views shown in Figs. 6 and 9 and Media 3 & 4. We would like to thank Manuel Aschwanden and Mark Blum (Optotune AG) for providing an ETL. Furthermore we thank Martin Wieckhorst for technical assistance. This work was supported by a grant to F.H. from the Swiss SystemsX.ch initiative (Project Neurochoice) and to J.H. by the Human Frontiers Science Program (HFSP). Furthermore, this work was funded by the Max Planck Society.

#192746 - $15.00 USD Received 24 Jun 2013; revised 13 Aug 2013; accepted 13 Aug 2013; published 30 Aug 2013